Title

Development of pulmonary blood flow evaluation method with a dynamic flat-panel detector (FPD): Quantitative correlation analysis with findings on perfusion scan

Abstract

Pulmonary blood flow is reflected in dynamic chest radiographs as changes in X-ray translucency, *i.e.*, pixel values. Thus, decreased blood flow should be observed as a reduction of the variation of X-ray translucency. We performed the present study to investigate the feasibility of pulmonary blood flow evaluation with a dynamic flat-panel detector (FPD). Sequential chest radiographs of 14 subjects were obtained with a dynamic FPD system. The changes in pixel value in each local area were measured and mapped on the original image by use of a gray scale in which small and large changes were shown in white and black, respectively. The resulting images were compared to the findings in perfusion scans. The cross-correlation coefficients of the changes in pixel value and radioactivity counts in each local area were also computed. In all patients, pulmonary blood flow disorder was indicated as a reduction of changes in pixel values on the mapping image, and a correlation was observed between the distribution of changes in pixel value and those in radioactivity counts ($0.7 \leq r$, 3 cases; $0.4 \leq r < 0.7$, 7 cases; $0.2 \leq r < 0.4$, 4 cases). The results indicated that the distribution of changes in

pixel value could provide a relative measure related to pulmonary blood flow. The present method is potentially useful for evaluating pulmonary blood flow as an additional examination in conventional chest radiography.

Key words: Chest radiography; Pulmonary blood flow; Functional imaging; Image analysis; Flat-panel detector (FPD)

1. Introduction

The lungs contain a constant volume of about 500 mL of blood, with 75 mL distributed variably across the vasculature due to cardiac pumping [1]. The variations in blood volume in the lungs are reflected on fluoroscopic images as changes in X-ray translucency [2-5]. Thus, pulmonary blood flow patterns can be evaluated by comparison of regional changes in X-ray translucency on the images. However, it is extremely difficult to evaluate slight changes in X-ray translucency by visual observation. Many reports have indicated the feasibility of pulmonary densitometry for quantifying these changes [6-9]. These methods have not been adopted for clinical use because of technical limitations, such as poor image quality and a small field of view (FOV) [10].

Dynamic flat-panel detectors (FPDs) allow acquisition of sequential chest

radiographs with a large FOV and high image quality. Whereas image-intensifier systems are now being replaced with FPD systems, they are also expected to be useful as a new type of functional imaging system. We have developed computerized methods for evaluating pulmonary blood flow based on the changes in pixel value both visually and quantitatively. Our previous study in which we used an FPD system indicated a linear relationship between changes in pixel value and those in blood volume [5]. Lung areas with small changes in pixel value were visually consistent with those showing blood flow defects, which were indicated on perfusion scans [11]. Although our method is expected to be useful as a new pulmonary functional imaging technique, quantitative and statistical evaluations have yet to be performed. In this study, to investigate the effectiveness of our method, we performed a quantitative assessment of the correlation between changes in pixel value by cardiac pumping measured in each local area and the findings on perfusion scans.

2. Materials and Methods

2-1 Subjects

Fourteen subjects were assessed in this study (39–82 years old; mean, 68 years old; M:F = 10:4). The subjects had been diagnosed with pulmonary diseases, such as emphysema,

pulmonary fibrosis, and bronchiolitis obliterans, based on clinical and examination findings that fulfilled the respective diagnostic criteria, such as findings on CT and pulmonary function tests. In addition, pulmonary blood flow disorder was diagnosed by lung perfusion scan. Approval for the study was obtained from our institutional review board, and the subjects gave their written informed consent for participation in the study.

2-2 Image acquisition

2-2-1 Dynamic chest radiography

Dynamic chest radiographs were obtained by use of an FPD system (Sonial Vision Safire II; Shimadzu, Kyoto, Japan). Thirty images were obtained in 4 s with exposure under the following conditions: 110 kV, 80 mA, 6.3 ms, source-to-image distance 1.5 m, 7.5 frames per second. Imaging was performed in the standing position, posteroanterior direction, with a rest expiratory level of breath-holding. The total entrance surface dose, measured in air without backscatter, was approximately 0.6 mGy, which was 1.5-fold greater than that in posteroanterior chest radiography determined as the guidance level by the International Atomic Energy Agency (IAEA) (0.4 mGy) [12]. The matrix size was 1440×1440 pixels, the pixel size was 260×260 μm, the FOV was 38×38 cm, and the

grayscale range of the images was 16 bits, which was proportional to the incident exposure in the FPD.

2-2-2 Perfusion scan

Perfusion scans were obtained in directions of 0°, 45°, 90°, 135°, 180°, 225°, 270°, and 315°, for 5 min per direction, by use of a gamma camera (E-CAM duet; Toshiba Medical, Tokyo, Japan) and ^{99m}Tc-MAA (200 MBq). The matrix size was 256×256 pixels, the pixel size was 1.95×1.95 mm, the FOV was 49.8×49.8 cm, and the grayscale range of the images was 8 bits, which was proportional to the radioactive isotope (RI) count. For comparison with the X-ray images, the average image was created from the anterior and mirror reversed posterior images.

2-3 Image analysis

Image analysis was performed on a personal computer (CPU, Pentium 4, 2.6 GHz; Memory, 2 GB; operating system, Windows XP; Microsoft, Redmond, WA) with our algorithm (Development environment, C++Builder; Borland, Scotts Valley, CA), for quantifying and visualizing slight changes in pixel value in the lung area (Fig. 1).

2-3-1 Preprocessing

For facilitating image analysis, images were reduced to 12 bits. Low pixel values were related to dark areas in the images, and these, in turn, were related to areas of high X-ray translucency in this study. The lung area was determined by edge detection by use of the first-derivative technique and an iterative contour-smoothing algorithm [13,14]. The hilar regions were excluded manually from the lung area. Areas outside the lung were assigned a value of zero. For determination of cardiac phase, the average pixel value was measured in the region of interest (ROI) located around the left ventricular wall throughout all frames, as shown in Fig. 2a [9,15]. Increases and decreases in pixel values were determined as the diastole phase and the systole phase, respectively (Fig. 2b). The frames composing a whole cardiac phase were selected.

2-3-2 Measurement of pixel values

Chest radiographs were divided into 72 × 72 blocks, 20 pixels on a side (Fig. 2a). The blocks located at the border were defined as the lung areas. We performed measurements in block units to reduce the influence of slight movement, dilation, and contraction of lung structures, and also to facilitate comparison of local changes and statistical analysis. The average pixel value $P_n(x, y)$ was measured in each block in the

lung areas, were x and y are the coordinates of blocks in the horizontal and vertical directions, respectively, and n is the frame number. $P_{ave}(x, y)$, the average pixel value of $P_n(x, y)$ in one cardiac cycle, was then calculated, and the differences between $P_n(x, y)$ and $P_{ave}(x, y)$ were determined throughout one cardiac cycle in each block, representing the difference from the average state in blood volume. The sum of the absolute differences was finally output as $P_{total}(x, y)$, representing the total changes in pixel values in each block in one cardiac cycle. $P_{ave}(x, y)$ and $P_{total}(x, y)$ are defined as follows:

$$P_{ave}(x, y) = [P_0(x, y) + P_1(x, y) + ... + P_n(x, y)]/N \quad (0 < n < N) \tag{1}$$

$$P_{total}(x, y) = \sum | P_n(x, y) - P_{ave}(x, y) | \ (0 < n < N), \tag{2}$$

where N is the number of frames in one cardiac cycle. The percentage of the results in each block to the summation of the results in all the blocks in lung areas was then calculated as,

$$P_{\%}(x, y) = \frac{P_{total}(x, y)}{\sum_{y=0}^{Y} \sum_{x=0}^{X} P_{total}(x, y)} \times 100, \tag{3}$$

where X and Y are the number of blocks in the horizontal and vertical directions, respectively; both were 72, and the computation was limited to lung areas in this study.

To facilitate visual evaluation, $P_{\%}(x, y)$ was mapped on the original image by use of a gray scale in which small changes were shown in white and large changes were shown in black (hereafter called the "Distribution map of $P_{\%}$") (Fig. 3a).

2-3-3 Image registration

The perfusion scan was transformed so that the matrix size and pixel size were adjusted to those of chest radiographs by linear interpolation. The transformed perfusion scan was made partially transparent and was overlaid on the chest radiograph. Then, image registration between the perfusion scan and the chest radiograph was performed manually by shifting and rotating based on the contour shape of the mediastinum, lung outline, and diaphragm.

2-3-4 Calculation of RI count

The perfusion scan was also divided into 72×72 blocks, 20 pixels on a side (Fig. 3b). The sum of pixel values was determined in each block. The percentage of total $RIcnt_{\%}$ was then calculated as follows:

$$RIcnt_{\%}(x,y) = \frac{RIcnt(x,y)}{\sum_{x=0}^{X}\sum_{y=0}^{Y} RIcnt(x,y)} \times 100, \quad (4)$$

where X and Y are the number of blocks in the horizontal and vertical directions, respectively; both were 72 in this study. In addition, x and y are the coordinates of the blocks in the horizontal and vertical directions, respectively. RI_{cnt} is the RI count measured in each block.

2-4 Statistical analysis

To examine the relationship between the results obtained with our method and those obtained by perfusion scan, we examined the null hypothesis that the regression line of $P_{\%}$–$RIcnt_{\%}$ had no gradient in each subject. The cross-correlation coefficients of $P_{\%}$–$RIcnt_{\%}$ were also computed [16].

3. Results

In all subjects, the null hypothesis was dismissed ($P=0.01$), and there was a correlation between $P_{\%}-RIcnt_{\%}$ ($0.7\leq r$, 3 cases; $0.4\leq r<0.7$, 7 cases; $0.2\leq r<0.4$, 4 cases). The maximum and minimum r values were 0.70 and 0.25, respectively. Figures 4–6 show the results for the subjects with strong ($0.7\leq r$), intermediate correlations ($0.4\leq r<0.7$), and weak correlations ($0.2\leq r<0.4$), respectively.

Figure 4 shows the results for a patient with pulmonary fibrosis (82-year-old man). The area surrounded by broken lines in the perfusion scan shows the area with reduced blood flow determined by a radiologist specializing in nuclear medicine (S.T.). The perfusion scan showed a marked reduction of blood flow in the left lung in comparison with the right lung (Fig. 4c). The distribution map of $P_{\%}$ also showed

reduced total changes in pixel value over the left lung (Fig. 4b). There was a strong correlation between $P_{\%}$ and $RIcnt_{\%}$ ($r=0.70$) (Fig. 4d).

Figure 5 shows the results for a patient with obstructive pulmonary disease (62-year-old man). The perfusion scan showed that there were areas of no blood flow in the upper right lung and of reduced blood flow in the left upper and middle lung (Fig. 5c). These areas showed reduced changes in pixel value in the distribution map of $P_{\%}$ (Fig. 5b). There was an intermediate correlation between $P_{\%}$ and $RIcnt_{\%}$ ($r=0.63$) (Fig. 5d).

Figure 6 shows the results in a patient with pleural adhesions in the left lung (74-year-old woman). The perfusion scan showed a reduction of blood flow over the whole left lung (Fig. 6c). However, the left lung did not show reduced changes in pixel value in the distribution map of $P_{\%}$ (Fig. 6b). The remaining area in the right lower lung showed reduced changes in pixel values. There was a weak correlation between $P_{\%}$ and $RIcnt_{\%}$ ($r=0.37$) (Fig. 6d).

4. Discussion

There was a good correlation between the findings in the distribution map of $P_{\%}$ and those in the perfusion scan in ten of the subjects. The results indicated that the

distribution map of $P_{\%}$ could provide relative measures related to pulmonary blood flow. Although the changes in pixel value do not indicate the absolute blood flow volume, the present method could be utilized for relative or temporal comparison in each patient rather than for inter-subject comparison.

However, there were four patients with a weak correlation between $P_{\%}$ and $RIcnt_{\%}$ ($r < 0.4$). This may have been due to differences in the items measured; lung scintigraphy measures nuclear radiation from a radiolabeled compound, *i.e.*, ^{99m}Tc-MAA, which is carried by blood flow, whereas the present method measures the changes in pixel value caused by blood flow and other factors, such as the movement of vessels and bronchi, and the dilation and contraction of vessels themselves. In three subjects with strong correlations, the other factors may little effect on the results. These factors may have been responsible for the differences in the results for the two cases shown in Fig. 4 ($r = 0.70$) and Fig. 6 ($r = 0.37$). Nevertheless, the findings in the perfusion scan were very similar. In addition, there may have been misregistration in the two images due to displacement of lung structures caused by differences in body posture and inspired volume during imaging. For example, the perfusion scan was performed in several minutes without breath holding in the supine position, whereas X-ray images were acquired at the end of exhalation in the standing position. Thus, the distribution map of

$P_{\%}$ did not show the same findings as the commonly used pulmonary perfusion method. In addition, in this study, manual registration between the perfusion scan and the chest radiograph might contribute to a poor correlation. Therefore, the results of the present study could not confirm that this technique has a sufficiently good diagnostic performance to replace the perfusion scan. Further studies with comparisons performed under the same conditions are required. For example, X-ray imaging in the supine position or expansion of this technique to 4-dimensional CT and comparison with SPECT-CT may address these problems. The diagnostic criteria and diseases for which the present method is applicable should also be determined in further studies in patients with the same diseases.

5. Conclusions

The feasibility of a pulmonary blood flow diagnostic imaging method with dynamic FPD was assessed. In 10 of 14 subjects, there was a correlation ($r > 0.4$) between the distribution of changes in pixel value during one cardiac cycle and those of the RI count measured in each local area, and a blood flow disorder was indicated as reduced changes in pixel value. However, four cases showed weak correlations, which was thought to be due to technical limitations and image misregistration. Although further studies are

required for the development of clinical implementation, the present method with real-time computer analysis is expected to be useful as an additional examination in conventional chest radiography.

References

[1] Hansen JT and Koeppen BM. Cardiovascular Physiology, In: Netter's Atlas of Human Physiology (Netter Basic Science). Teterboro, New Jersey: Icon Learning Systems; 2002.

[2] Heyneman LE. The chest radiograph: Reflections on cardiac physiology. Radiological Society of North America. Scientific Assembly and Annual Meeting Program 2005, 2005;145.

[3] Felson B. Chest roentgenology. Philadelphia, London, Toronto: W B Saunders Co.; 1973.

[4] Goodman LR. Felson's Principles of Chest Roentgenology. a programmed text, 3rd ed. Philadelphia, London, Toronto: W B Saunders Co.; 2006.

[5] Tanaka R, Sanada S, Fujimura M, Yasui M, Nakayama K, Matsui T, Hayashi N, Matsui O. Development of functional chest imaging with a dynamic flat-panel detector (FPD). Radiological physics and technology. 2008;1:137-143.

[6] Silverman NR. Clinical video-densitometry. Pulmonary ventilation analysis. Radiology. 1972;103:263-265.

[7] Silverman NR, Intaglietta M, Tompkins WR. Pulmonary ventilation and perfusion during graded pulmonary arterial occlusion. J Appl Physiol. 1973;34:726-731.

[8] Bursch JH. Densitometric studies in digital subtraction angiography: assessment of pulmonary and myocardial perfusion. Herz. 1985;10:208-214.

[9] Liang J, Jarvi T, Kiuru A, Kormano M, Swedstrom E. Dynamic chest image analysis: model-based perfusion analysis in dynamic pulmonary imaging. J Applied Signal Process. 2003;5:437-448.

[10] Fujita H, Doi K, MacMahon H, Kume Y, Giger ML, Hoffmann KR, Katafuchi T, Ohara K, Chan HP. Basic imaging properties of a large image intensifier-TV digital chest radiographic system. Invest Radiol. 1987;22:328-335.

[11] Tanaka R, Sanada S, Fujimura M, Yasui M, Tsuji S, Hayashi N, Nanbu Y, Matsui O.

Pulmonary blood flow evaluation using a dynamic flat-panel detector: Feasibility study with pulmonary diseases. IJCARS. 2009;4:449-445.

[12] International basic safety standards for protection aginst ionizing radiation and for the safety of radiation sources. Vienna; International atomic energy agency (IAEA): 1996.

[13] Xu XW, Doi K. Image feature analysis for computer-aided diagnosis: accurate determination of ribcage boundary in chest radiographs. Med Phys. 1995;22:617-626.

[14] Li L, Zheng Y, Kallergi M, Clark RA. Improved method for automatic identification of lung regions on chest radiographs. Acad Radiol. 2001;8:629-638

[15] Myers PH, Nice CM, Becker HC, Nettleton WJ, Sweeney JW, Meckstroth GR. Automated computer analysis of radiographic images, Radiology, 1964;83:1029-1033.

[16] Rees D. Essential Statistics 4th ed. (Text in statistical science) Florida: Chapman & Hall; 2001.

Figure captions

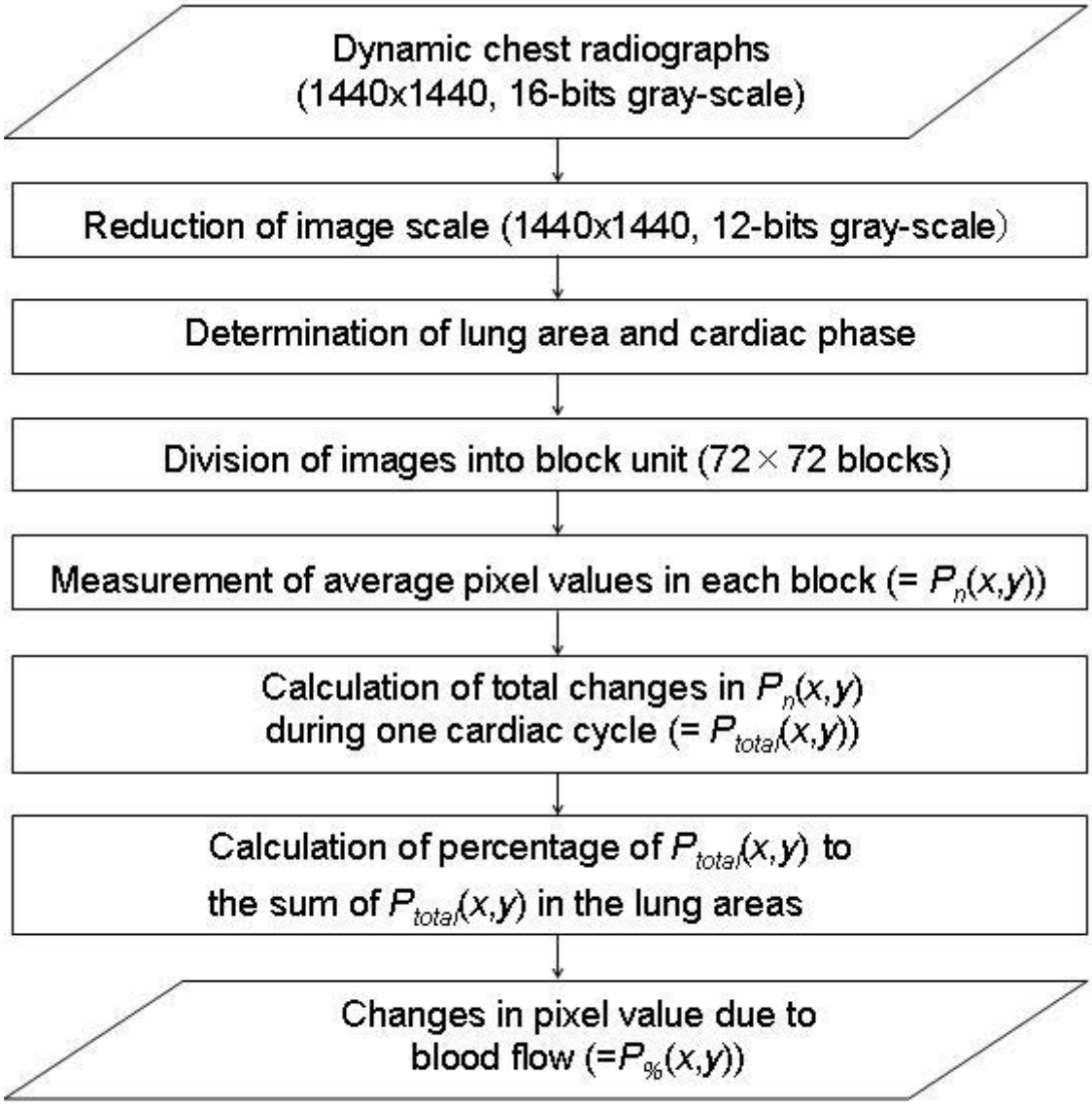

Fig. 1 Overall scheme of our algorithm

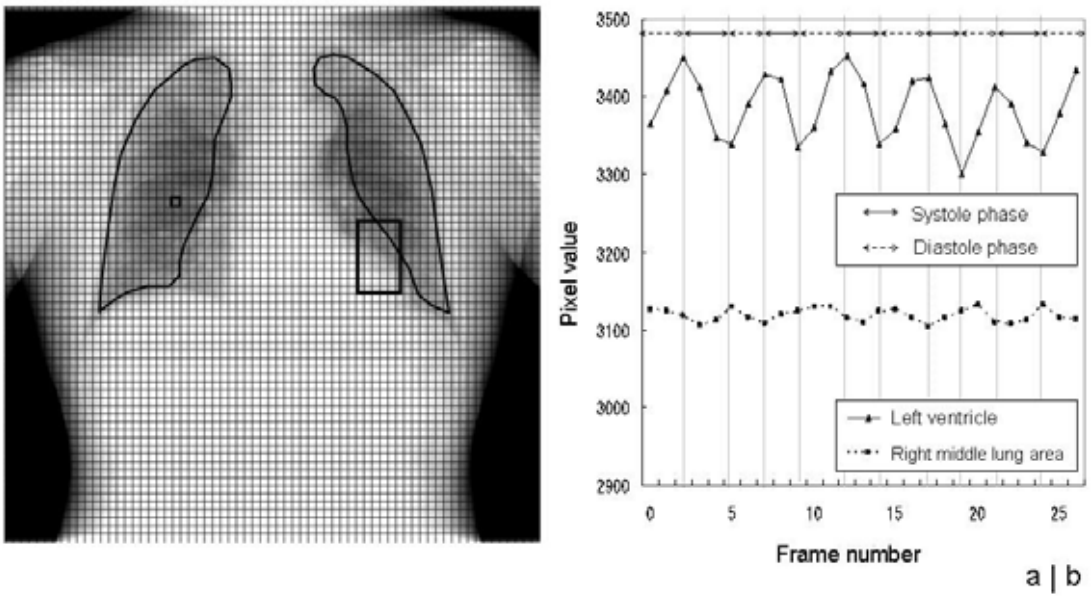

Fig. 2 (a) One frame of dynamic chest radiograph (emphysema, 58-year-old man). The black bold lines show the lung area recognized, and the grid lines show the unit of measurement for the local average pixel value. The large square shows the region of interest (ROI) located around the left ventricular wall for determining the cardiac phase. (b) Relationship between average pixel values measured in the ROI located around the left ventricular wall and one block in the right middle lung area.

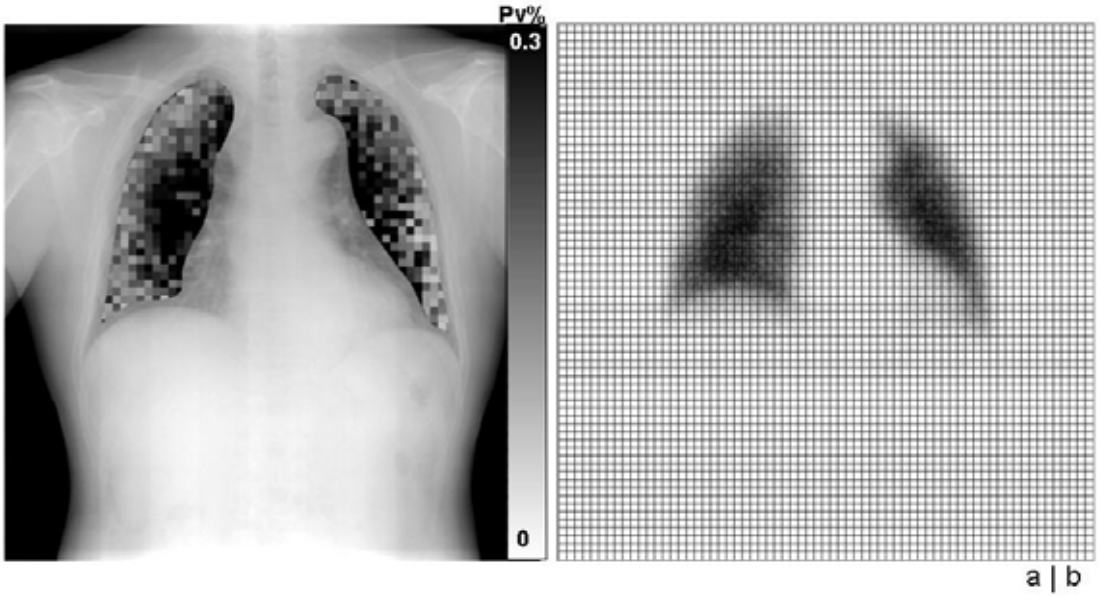

Fig. 3 (a) Distribution map of $P_{\%}$, and (b) perfusion scan divided into blocks (emphysema, 58-year-old man).

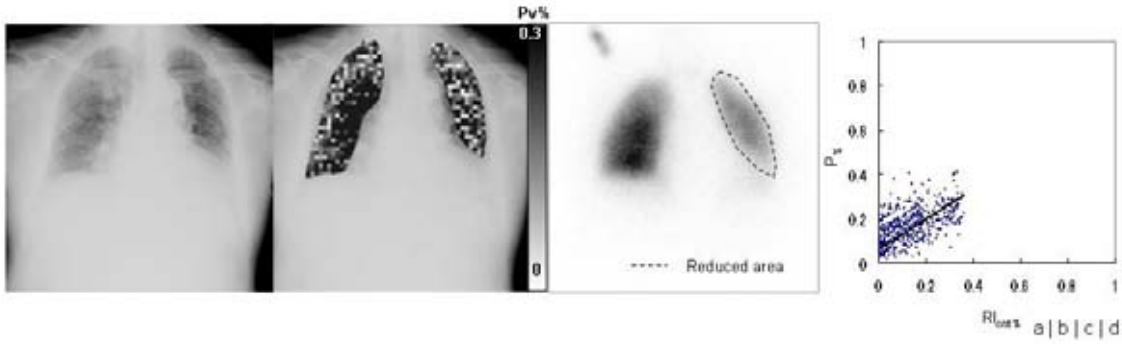

Fig. 4 Results in restrictive lung disease (pulmonary fibrosis, 82-year-old man). (a) One frame of dynamic chest radiograph. (b) Distribution map of $P_{\%}$. (c) Lung perfusion scan (^{99m}Tc-MAA). The area surrounded by broken lines shows reduced blood flow. (d) Scatter diagram of $P_{\%}$–$RIcnt_{\%}$ ($r = 0.70$) The regression line is shown.

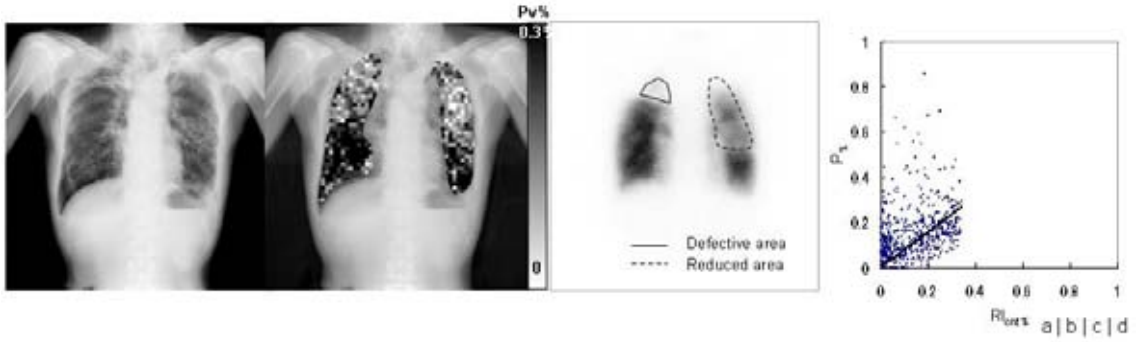

Fig. 5 Results in obstructive pulmonary disease (bronchiolitis obliterans with upper-lobe fibrosis and pneumothorax in the right lower lung, 62-year-old man). (a) One frame of dynamic chest radiograph. (b) Distribution map of $P_{\%}$. (c) Lung perfusion scan (^{99m}Tc-MAA). The areas surrounded by solid and broken lines show reduced blood flow. (d) Scatter diagram of $P_{\%}$–$RIcnt_{\%}$ (r=0.63). The regression line is shown.

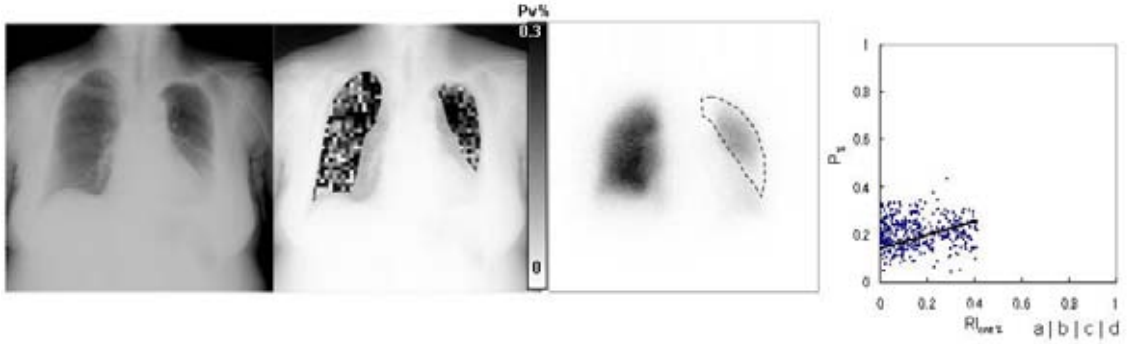

Fig. 6 Results in restrictive lung disease (pleural adhesions in the left lung, 74-year-old woman). (a) One frame of dynamic chest radiograph. (b) Distribution map of $P_{\%}$. (c) Lung perfusion scan (^{99m}Tc-MAA). The area surrounded by broken lines shows reduced blood flow. (d) Scatter diagram of $P_{\%}$–$RIcnt_{\%}$ (r=0.37). The regression line is shown.